

## INDENTATION DEFORMATION/FRACTURE OF NORMAL AND ANOMALOUS GLASSES

A. ARORA, D.B. MARSHALL, B.R. LAWN

*Department of Applied Physics, School of Physics, University of New South Wales, Kensington, N.S.W. 2033, Australia*

and

M.V. SWAIN

*Service Central de Recherche, Saint-Gobain Industries, 39 Av. Lucien Lefranc, 93304 Aubervilliers Cedex, France*

Received 26 September 1978

Vickers deformation/fracture indentations have been investigated in six silicate glasses. The characteristic damage patterns fall into two distinct groups, according to whether the glass shows “normal” or “anomalous” mechanical behaviour. Observations of the damage morphology during and after contact, of the scales of the deformation and fracture zones, and of the residual stress intensity about the impressions, all point to a basic difference in the local stress/strain micromechanics. This difference is discussed in relation to the factors which control the brittleness of glass.

### 1. Introduction

It is now well established that silica-rich glasses exhibit certain anomalous behaviour in their mechanical and thermal properties [1–3]. Fused silica is the classic example of the so-called “anomalous” glasses. Glasses with a substantial component of network modifiers in their structure behave more “normally”, i.e. as typified by most crystalline solids. It is generally accepted that the explanation of anomalous behaviour rests with the tetrahedral bond structure of the basic silica network, in particular with the relative movements of atoms in the Si–O–Si linkages; modifying ions are seen as restricting these movements.

This distinction between normal and anomalous behaviour extends to the deformation [4–9] and fracture [10,11] properties of glasses. The aim in the present work is to investigate the effect of glass composition on basic deformation/fracture parameters, using an indentation technique. Based on the principles of indentation fracture mechanics [12], our study considers the micromechanics of

crack development within a geometrically similar, deformation-controlled contact field [13–15]. The results obtained will be seen to follow the normal/anomalous dichotomy, pointing to some basic difference in the nature of the indentation process.

## 2. Indentation experiments

### 2.1. Materials and test procedure

The glasses studied were in the form of microscope slides  $75 \times 25 \times 1.5$  mm, from the same source as the specimens used by Wiederhorn and co-workers to fabricate test pieces in their fracture mechanics studies [10,16]. Table 1 shows the compositions of the glasses. Each slide had been pre-annealed, silica excepted, to remove residual stresses.

Indentations were made with a Vickers diamond pyramid, over a load range 0.1–100 N. A dry nitrogen test environment minimized kinetic effects in the indentation micromechanics. Each glass surface could accommodate several hundred such indentations without any detectable interaction between neighbours.

### 2.2. Deformation/fracture morphology

Examination of the indentation damage by optical microscopy showed a clear distinction between the normal and anomalous glasses. Some of the features to be described here have been noted in other studies [17–22]. We concentrate on those details which highlight the differences in the two glass types. Basically, the normal glasses were characterized by well-defined, classic sharp-indenter patterns, whereas the anomalous glasses showed somewhat more complex configurations. Typical patterns are shown in figs. 1 and 2, with soda-lime and silica glasses taken as representative of normal and anomalous types respectively.

Table 1

Composition (weight fraction) of glasses studied. (After [10,16].) *N* denotes normal, *A* denotes anomalous

Glass	Type	SiO <sub>2</sub>	B <sub>2</sub> O <sub>3</sub>	Al <sub>2</sub> O <sub>3</sub>	Na <sub>2</sub> O	K <sub>2</sub> O	MgO	CaO	PbO
Silica	A	0.998							
96% silica	A	0.96	0.03	0.01					
Borosilicate	A	0.80	0.14	0.02	0.04				
Soda-lime	N	0.72		0.02	0.14	0.01	0.04	0.07	
Lead-alkali	N	0.60		0.04	0.10	0.02			0.24
Aluminosilicate	N	0.57	0.04	0.20	0.01		0.12	0.06	

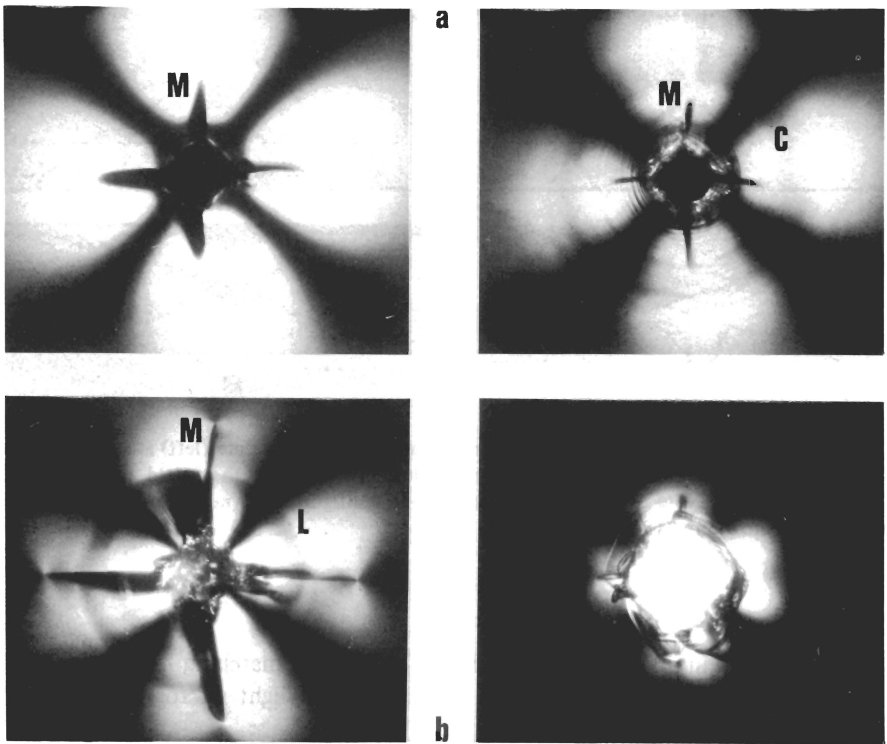


Fig. 1. Polarized light micrographs of Vickers indentations in soda-lime (left) and silica (right) glasses, taken *in situ* from beneath contact zone (central dark square): (a) full load ( $P = 40$  N), (b) complete unload. Optical contrast from median/radial ( $M$ ) cracks exceeds that from cone ( $C$ ) or lateral ( $L$ ) cracks, owing to near-edge-on orientation with respect to light beam. Width of field  $600\ \mu\text{m}$ . Note relatively small residual birefringence in silica specimen.

The first method of observation was aimed at following the entire evolutionary sequence of the indentation deformation/fracture patterns. It has already been established [19] that the unloading half-cycle is of no less importance than the loading half-cycle in generating a driving force for the cracks, due to the development of residual stresses about the deformation zone [23,24]. The indentation process was carried out *in situ* on the stage of an inverted microscope, and viewed from below in polarized light [25,26]. Fig. 1 shows indentations observed in this way at maximum load and complete unload. In contrasting the two types of pattern in these micrographs, special note may be made of the relatively weak residual stress birefringence in the anomalous glass.

The second method of observation provided a closer look at events in the immediate vicinity of the deformation zone. Some of the glass slides were pre-cracked, and indentations made across the crack trace immediately behind the arrested tip.

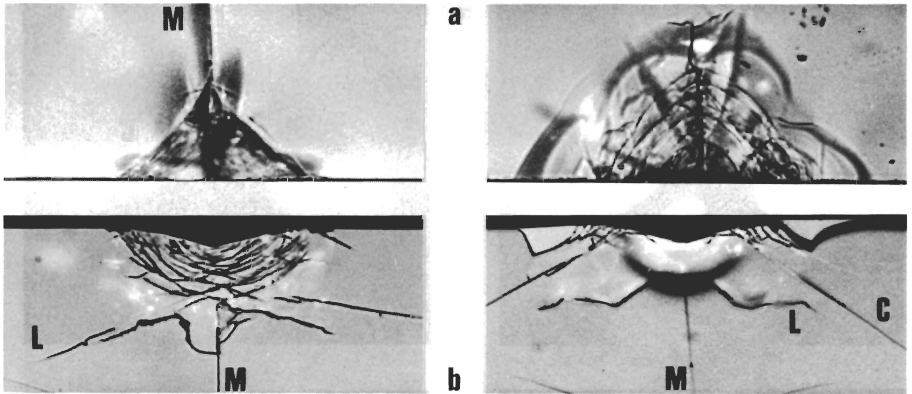


Fig. 2. Reflected light micrographs of Vickers indentations in soda-lime (left) and silica (right) glasses: (a) half-surface, (b) section, views. Indentation load 30 N. Width of field 220  $\mu\text{m}$ . Crack labelling as in fig. 1. Note different deformation zone configurations (near-semi-circular region immediately below impression) in (b).

Subsequent breaking of the slides produced convenient matching half-surface and section views of the contact damage [22]. Reflected light micrographs of such views are shown in fig. 2.

From the optical observations we identify the following sequences of events for normal and anomalous glasses:

### 2.2.1. Normal glasses.

Loading half-cycle: (a) at low loading the deformation processes in the region of high shear and compression immediately below the contact generate incipient flaw nuclei, the remnants of which are seen in fig. 2 (left) running approximately parallel to the zone boundaries [22]; (b) at some threshold one or more of these flaws reach a critical size, and grow into small, subsurface, penny-like “median” cracks on tensile symmetry planes defined by the load axis and an impression diagonal [14,19]; (c) on further loading, the contact continues its expansion and drives the median cracks stably downward into the glass, giving rise to the characteristic star pattern in fig. 1a (left). Unloading half-cycle: (d) on load reversal, mismatch stresses associated with stress/strain incompatibility between deformation zone and surrounding elastic matrix begin to dominate the applied field, thereby driving the medians further outward and upward toward the specimen surface, fig. 1b (left); (e) on approaching completion of the cycle the residual stresses begin to dominate the field, and drive sideways-spreading, saucer-like “lateral” cracks from within the deformation zone, fig. 1b (left) [23]. Some variants occur in this somewhat idealized pattern of behaviour, notably at low loads: even if the threshold stage (b)

is not attained during the loading half-cycle the residual stress field may become sufficiently intense to initiate and drive near-surface "radial" cracks outward from impression corners as the indenter is withdrawn, thereby producing a final surface crack configuration to all intents and purposes identical to that of fig. 1b (left).

### 2.2.2. *Anomalous glasses.*

Loading half-cycle: (a) at low loads the deformation processes again activate flaw nuclei, particularly at or about the surface zone boundary, figs. 1 and 2 (right); (b) at threshold a critical nucleus grows unstably from the surface into a "ring" crack about the impression, with more or less classical Hertzian geometry [12]; (c) at increasing load the ring crack propagates stably downward until its surface trace is encompassed within the expanding contact, whence a new ring initiates, until ultimately a multiple system of steeply penetrating "cone" cracks obtains; at the same stage in the loading variable median/radial and lateral cracking may occur, but in a manner severely restricted by the preceding cone cracks, fig. 1a (right). Unloading half-cycle: (d) load reversal produces little change in the cone/median/radial crack configuration; (e) as unloading completes, a collar of material often detaches from part way down one or more of the cones to leave an annular surface crater, especially in heavily loaded surfaces, fig. 1b (right). In exceptional cases, where the cone initiation stage (b) is for some reason suppressed, a reasonably well-developed median crack system can be realized — however, even then the radial surface traces tend to be irregular, often emanating well away from the impression corners, and residual-stress driven extension during unloading remains slight.

The major conclusion to be drawn here, echoed by similar observations on all the glasses listed in table 1, is that the processes responsible for initiating the fracture patterns are quite different in the normal and anomalous glasses. This in turn implies a difference in the deformation mechanisms themselves, bearing in mind that the geometrical conditions of indentation (*viz.* rigid pyramid indenter; flat, isotropic, homogeneous specimen) are essentially invariant. We shall look more closely at the influence of glass structure on the mode of deformation in the Discussion.

### 2.3. *Parameters of the deformation/fracture patterns*

An attempt was made to relate the scales of the deformation and fracture zones in the indented glasses to basic brittleness parameters. In accordance with the scheme outlined in recent indentation fracture analyses [13–15] the idealized median crack geometry of fig. 3 was taken as the basis for measurement. As we have just seen, crack patterns closely following this geometry are the rule in normal glasses, but the exception in anomalous glasses. Data in the latter case are therefore somewhat limited and variable.

For present purposes it is necessary only to summarize the essential details of the deformation/fracture mechanics. In the case of the deformation zone the

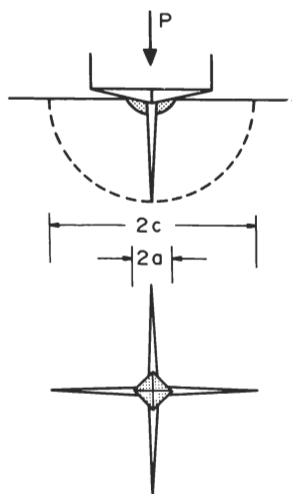


Fig. 3. Parameters of well-developed deformation/median-crack system at Vickers indentation.

characteristic dimension  $a$  of the impression relates to the load  $P$  via the hardness  $H$ :

$$P/a^2 = \alpha_0 H = \text{constant} . \quad (1)$$

Measurements investigating this relation are generally taken in the deformation-controlled region of behaviour  $c < a$ , but the incidence of cracking does not appear to influence the deformation mechanics, as long as the impression remains reasonably well defined. Taking  $a$  as the impression half-diagonal as in fig. 3, and defining hardness in terms of the mean indentation pressure over the projected contact area (not the actual contact area, as conventionally used in defining the Vickers hardness number), we have  $\alpha_0 = 2$ . For the crack pattern the analogous equation is given in terms of the fracture toughness  $K_{Ic}$ :

$$P/c^{3/2} = \beta_0 K_{Ic} = \text{constant} . \quad (2)$$

Crack measurements are usually made in the region  $c \gg a$ , where the median system is considered to be well-developed [13]. Uncertainties in the fracture mechanics preclude a theoretical estimate of the numerical constant  $\beta_0$  to within much better than a factor of two or three, and an empirical adjustment becomes necessary.

In discussing how an indentation pattern of the type modelled in fig. 3 reflects on the brittleness characteristics of a material, Lawn and Marshall [15] point out that data representing eq. (1) and (2), suitably normalized, may be conveniently

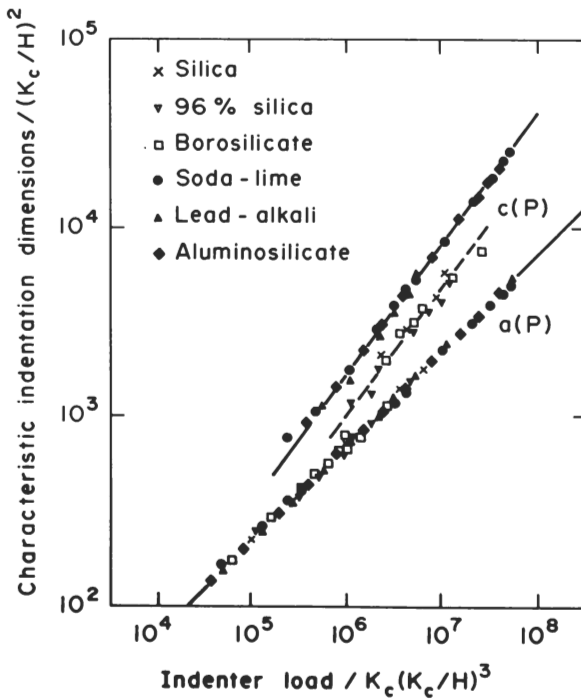


Fig. 4. "Universal" deformation/fracture diagram showing indentation data plotted for normal and anomalous glasses.

Table 2

Hardness and toughness of glasses studied <sup>a)</sup>

Glass	<i>H/GPa</i>	<i>K<sub>c</sub>/MPa m<sup>1/2</sup></i>
Silica	7.6	0.79
96% silica	6.9	0.72
Borosilicate	6.1	0.76
Soda-lime	5.6	0.75
Lead-alkali	4.9	0.68
Aluminosilicate	6.6	0.91

<sup>a)</sup> Hardness data from present study, measurement error  $\pm 5\%$ . Toughness data from ref. [10], error  $\pm 2\%$ .

plotted on a single, "universal" deformation/fracture diagram. Such a plot is shown in fig. 4 for all the glasses under consideration in the present study: using the appropriate values of  $H$  and  $K_c$  listed in table 2, load is normalized in terms of  $K_c(K_c/H)^3$  and linear dimensions in terms of  $(K_c/H)^2$  to produce dimensionless test variables. It is clear from the fracture data that the value of  $\beta_0$  for the anomalous glasses differs significantly from that for the normal glasses. Physically,  $\beta_0$  can be regarded as a geometrical factor which relates the normal indentation force to the effective centre-loading force driving the penny-like median cracks [27]: a variation in this quantity accordingly implies a difference in the near-contact deformation mechanisms responsible for redistributing the applied loading.

#### 2.4. Stress birefringence measurements

The classification of the deformation/fracture characteristics noted above into two distinctive groupings prompted a closer look at the residual stresses about the indentation sites. Evidence exists that residual-stress effects can be significant in the indentation fracture mechanics [28,29], and we have already made special mention of the marked difference in behaviour shown by normal and anomalous glasses during the unloading half-cycle. A standard optical birefringence technique was therefore used to provide a comparative measure of stress levels in the tested slides. The indentations were viewed normal to the plate between crossed polars, and a compensator used to determine the retardation close to the impression sides, where the birefringence was a maximum. As with the hardness data, the incidence of cracking appeared to have little effect on the results.

It is readily demonstrated that the birefringence measurements contain quantitative information on the residual stress field. The retardation is defined as

$$\Gamma = \int_0^t \Delta n(z) dz \quad (3)$$

where  $\Delta n$  is the birefringence, i.e. the difference in the principal refractive indices perpendicular to the optical path, here integrated over the plate thickness  $t$ . Now the birefringence relates directly to the corresponding differences in principal stresses (by symmetry, directed parallel and perpendicular to the impression sides)  $\Delta\sigma$ , via the stress-optical coefficient  $A$ , such that

$$\Gamma = A \int_0^t \Delta\sigma(z) dz . \quad (4)$$

Since the spatial extent of the field must scale with the impression half-diagonal  $a$ , and the intensity of the field likewise with the hardness  $H$ , eq. (4) may be conveniently normalized to give

$$\Gamma = AHa \int_0^{t/a} [\Delta\sigma(z/a)/H] d(z/a) . \quad (5)$$

Eq. (1) may be used to eliminate  $a$ :

$$\Gamma = \eta AH^{1/2}P^{1/2} \quad (6)$$

where we define the dimensionless quantity

$$\eta = \alpha_0^{-1/2} \int_0^{t/a} [\Delta\sigma(z/a)/H] d(z/a). \quad (7)$$

We may note that the constancy of  $\eta$  rests with geometrical similitude in the residual field.

Analysis of the birefringence measurements was carried out in accordance with eq. (6). First, the stress-optical coefficient for each glass was determined from a routine calibration test, in which a known uniaxial stress was applied along the diameter of a disc-shaped test piece and the resultant birefringence measured along the disc axis [30]: the values are listed in table 3. The experimental data were then plotted as  $\Gamma A^{-1}H^{-1/2}P^{-1/2}$  against load, fig. 5. Each glass gives a horizontal plot, confirming indentation similarity with load, but the data again fall into two distinct groups. The level of residual stress, as reflected in the integral of eq. (7), is clearly smaller for the anomalous glasses, consistent with the crack morphology observations.

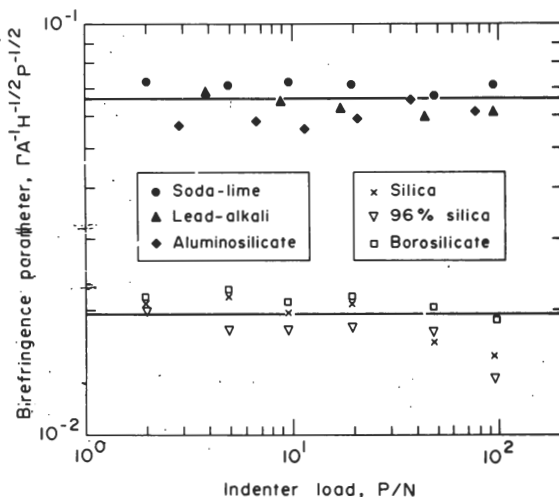


Fig. 5. Birefringence data for residual Vickers impressions in normal and anomalous glasses. Horizontal lines represent best fits to the two data groups. Measurement error in ordinate variable  $\pm 0.005$ .

Table 3  
Stress-optical coefficients of glasses studied a)

Glass	$A/(TPa)^{-1}$
Silica	3.53
96% silica	3.90
Borosilicate	3.83
Soda-lime	2.65
Lead-alkali	3.03
Aluminosilicate	2.68

a) Measurement error  $\pm 2\%$ .

### 3. Discussion

#### 3.1. Anomalous properties of glasses

Our study reveals basic differences in the indentation deformation/fracture behaviour of normal and anomalous glasses. A survey of the structural characteristics of fused silica and its modifications [1–3] shows that these differences correlate with a number of other mechanical and thermal properties. In particular, anomalous glasses are distinguished by an unusually low coefficient of thermal expansion (negative at low temperatures), and a positive temperature gradient and negative pressure gradient of bulk modulus. These are properties which are highly structure-sensitive, suggestive of a strong dependence on the spatial arrangement of the silica tetrahedra. The observation of similar anomalous behaviour in other tetrahedrally-coordinated glasses [e.g.  $GeO_2$ ,  $BeF_2$ ,  $Zn(PO_3)_2$ ] but not in glasses with threefold coordination (e.g.  $B_2O_3$ ) [31] reinforces this conclusion. Most workers agree that the transverse bending or vibrational modes of the Si–O–Si linkages between the network tetrahedra play a dominant role in the anomalous behaviour of fused silica, with network modifying ions in the interstices of the structure inhibiting these modes in the normal glasses: however, the detailed mechanism of structural response to stress or temperature remains a matter of some contention.

Of special relevance here is the role of such structural features in the deformation properties of silicate glass. Because of its brittleness, glass is not readily amenable to conventional mechanical testing methods; there is a tendency to spontaneous failure before any deformation mode can manifest itself in the stress/strain response. Techniques which involve large components of hydrostatic compression to inhibit fracture are therefore necessary. It is in this context that the indentation test is currently arousing considerable interest in the study of brittle materials: the contact field is primarily one of compression and shear (although not entirely free of tension, as evidenced by the indentation cracking), thereby allowing for

controlled production and study of irreversible deformation. Thus, following earlier studies of the residual impressions left by sharp indenters in a variety of glass compositions [32,33], Marsh [34] concluded that the deformation of glass is essentially plastic in nature. Subsequent workers, notably Neely and Mackenzie [7] and Ernsberger [8], citing results from high-pressure "belt" apparatus [4-6], argued in favour of a densification mode, especially in pure fused silica; Ernsberger's study, in particular, produced definitive evidence for the existence of densified material about indentation sites, although he could not refute the possibility that plastic flow accompanies the compaction. Peter [35], in detailed microscopic investigations of the indentation topography, noted a transformation from essentially radial to lateral ("pile-up") displacement of material about the indenter as the modifier content was increased, suggesting a corresponding transformation from densification to plasticity in the deformation mechanism. There is an implication here that normal glasses deform largely by a shear-dominated flow process, which is necessarily *reconstructive* in the bond configuration (i.e. bonds must be continually broken and remade with new neighbours), whereas anomalous glasses deform by a pressure-dominated densification process, thought to be basically *displacive* (as indicated by the recovery of the impression on annealing [6]). The role of modifying ions in the structure is then seen as one of providing "easy-slip" paths through an otherwise rigid, strongly covalent network [36]. Details of the actual mechanisms, however, remain obscure.

No less obscure than the mechanisms of deformation in glasses are the mechanisms of fracture. Wiederhorn and co-workers [10,11] have identified basic differences in the fracture behaviour of normal and anomalous glasses, and have considered possible explanations of these differences in terms of the way the network structure responds in the region of intense tensile stress at the tip of a propagating crack. Bearing in mind the signs of the pressure gradients of bulk modulus in the two glass types, one may expect the stiffness of the structure to be locally depressed in the crack-tip region for normal glasses, and correspondingly enhanced for anomalous glasses. This could account for a relatively high ratio of fracture energy to elastic modulus observed for anomalous glasses [10], fracture energy (hence toughness) relating explicitly to conditions within the crack-tip zone [37]. It is also suggested [11] that such structural conditions could explain the fact that the normal glasses show intrinsic slow crack growth in vacuum, whereas the anomalous glasses do not: however, the role of modifying ions in assisting crack-tip bond rupture in the former case has yet to be fully clarified, making it difficult to come to any definitive conclusion concerning crack-tip processes.

### 3.2. *Indentation deformation/fracture behaviour*

We are now in a position to place some physical interpretation on the indentation results reported in section 2. The invariance of the indenter/specimen contact geometry in the Vickers test arrangement leads us to conclude that the normal and

anomalous glasses must differ in some fundamental way in their stress/strain response. Unfortunately, there exists no detailed comparative stress analysis of the sharp-contact problem for materials which deform by competing flow and densification modes, although some semi-empirical calculations have recently been attempted [24,38]. Difficulties in this type of analysis include the precise form of the appropriate constitutive relations, the boundary conditions at the indenter/specimen interface, and the presence of the free surface outside the contact area (ignored, for instance, in "expanding cavity" models). Nevertheless, one may draw certain inferences concerning the driving forces for the attendant fracture from the evidence presented here for a comparatively small residual stress effect associated with indentations in the anomalous glasses:

### 3.2.1. Crack initiation.

The nature of the deformation-induced crack nuclei responsible for the ultimate indentation fracture patterns must reflect strongly on the deformation processes themselves. Our residual-stress observations lend support to the contention that the mode of deformation transforms from reconstructive flow-dominated to displacive densification-dominated as one goes from network-modified to more open silica-rich glasses [6,35]. Accordingly, in normal glasses flaws generate on planes of apparent shear displacement within the subsurface contact zone, as in fig. 2 (left) [22]. In anomalous glasses, on the other hand, generation occurs preferentially in the near-surface regions immediately surrounding the compacted contact zone, where local enhancement of tensile stresses is expected, fig. 2 (right). This difference in flaw mechanism would explain the tendency to median-crack formation in the normal glasses, cone-crack formation in the anomalous glasses.

### 3.2.2. Crack propagation.

Once developed, the indentation cracks propagate according to some fracture mechanics relation  $c(P)$ . In our analysis of the median/radial crack system the distinction between anomalous and normal glasses is marked by a shift in the data representing this relation on the universal plot of fig. 4. We have already indicated (section 2.2) that such a data shift can be accommodated only by a change in the indentation constant  $\beta_0$  in eq. (2); it cannot, for instance, be accommodated by any anomaly in  $K_c$ , as might be inferred from Wiederhorn's toughness data [10], since variations in this parameter simply displace the fracture data along the normal curve. A systematic change in  $\beta_0$  can in fact arise from residual-stress effects: a proper analysis leading to eq. (2) incorporates stress intensity factors representing an applied field based on purely elastic contact plus a residual field arising from elastic/inelastic mismatch [39], and omission of the second term effectively results in an overestimate in  $\beta_0$ . Quantitative estimates from fracture mechanics studies of indentation cracking in soda-lime glass [39] indicate an increase by a factor  $\approx 1.8$ , whereas a factor  $\approx 2.1$  is needed to account for the shift in fig. 4. It is likely that other factors contribute to this effect, for example the constraint of

dominant cone cracks on the expanding radial cracks in the anomalous glasses, but this is not easily quantified.

The conclusions drawn in this study bear on a number of important fracture-related technological problems. Indentation mechanics is currently being adopted as a basis for analysing strength degradation, surface erosion, wear, grinding and abrasion, etc in brittle materials [12], and [40–42]. Analyses of this type generally begin with the assumption of model indentation deformation/fracture system, geometrical similitude providing the cornerstone for mathematical formulation. It is apparent from the present results that inter-comparisons of predicted properties for different material types need to be made with due caution.

### Acknowledgements

Partial funding of this project was provided by the Australian Research Grants Committee. S.M. Wiederhorn kindly provided the glass specimens.

### References

- [1] O.L. Anderson and G.J. Dienes, in: *Non-Crystalline Solids*, ed. V.D. Frechette (Wiley, New York, 1960) p. 449.
- [2] R. Bruckner, *J. Non-Crystalline Solids* 5 (1970) 123.
- [3] M.R. Vukcevic, *J. Non-Crystalline Solids* 11 (1972) 25.
- [4] P.W. Bridgman and I. Simon, *J. Appl. Phys.* 24 (1953) 405.
- [5] H.M. Cohen and R. Roy, *J. Am. Ceram. Soc.* 44 (1961) 523.
- [6] J.D. Mackenzie, *J. Am. Ceram. Soc.* 46 (1963) 461, 470.
- [7] J.E. Neely and J.D. Mackenzie, *J. Mat. Sci.* 3 (1968) 603.
- [8] F.M. Ernsberger, *J. Am. Ceram. Soc.* 51 (1968) 545.
- [9] S. Sakka and J.D. Mackenzie, *J. Non-Crystalline Solids* 1 (1969) 107.
- [10] S.M. Wiederhorn, *J. Am. Ceram. Soc.* 52 (1969) 99.
- [11] S.M. Wiederhorn, H. Johnson, A.M. Diness and A.H. Heuer, *J. Am. Ceram. Soc.* 57 (1974) 336.
- [12] B.R. Lawn and T.R. Wilshaw, *J. Mat. Sci.* 10 (1975) 1049.
- [13] B.R. Lawn, T. Jensen and A. Arora, *J. Mat. Sci.* 11 (1976) 573.
- [14] B.R. Lawn and A.G. Evans, *J. Mat. Sci.* 12 (1977) 2195.
- [15] B.R. Lawn and D.B. Marshall, *J. Am. Ceram. Soc.*, in press.
- [16] S.M. Wiederhorn and L.H. Bolz, *J. Am. Ceram. Soc.* 53 (1970) 543.
- [17] K.W. Peter, *Glasstech. Ber.* 37 (1964) 333.
- [18] L.G. Baikova, V.P. Pukh and S.N. Talalakin, *Sov. Phys. Solid State* 15 (1974) 1437.
- [19] B.R. Lawn and M.V. Swain, *J. Mat. Sci.* 10 (1975) 113.
- [20] A.G. Evans and T.R. Wilshaw, *Acta Met.* 24 (1976) 939.
- [21] K. Phillips, G.M. Crimes and T.R. Wilshaw, *Wear* 41 (1977) 327.
- [22] M.V. Swain and J.T. Hagan, *J. Am. Ceram. Soc.*, in press.
- [23] B.R. Lawn, M.V. Swain and K. Phillips, *J. Mat. Sci.* 10 (1975) 1236.
- [24] C.M. Perrott, *Wear* 45 (1977) 293.
- [25] J.S. Williams, B.R. Lawn and M.V. Swain, *Phys. Stat. Solidi (a)* 2 (1970) 7.

- [26] V.R. Howes, *Glass Tech.* 15 (1974) 148.
- [27] B.R. Lawn and E.R. Fuller, *J. Mat. Sci.* 10 (1975) 2016.
- [28] M.V. Swain, *J. Mat. Sci.* 11 (1976) 2345.
- [29] J.J. Petrovic, R.A. Dirks, L.A. Jacobson and M.G. Mendiratta, *J. Am. Ceram. Soc.* 59 (1976) 177.
- [30] J.W. Dally and W.F. Riley, *Experimental Stress Analysis* (McGraw-Hill, New York, 1965), ch. 8.
- [31] C.R. Kurkjian, J.T. Krause, H.J. McSkimin, P.A. Deatch and T.B. Bateman, in: *Amorphous Materials*, eds. R.W. Douglas and B. Ellis (Wiley-Interscience, New York, 1972), p. 463.
- [32] E.W. Taylor, *J. Soc. Glass Tech.* 34 (1950) 69.
- [33] L. Ainsworth, *J. Soc. Glass Tech.* 38 (1954) 479, 501, 536.
- [34] D.M. Marsh, *Proc. Roy. Soc. Lond.* A279 (1964) 420.
- [35] K.W. Peter, *J. Non-Crystalline Solids* 5 (1970) 103.
- [36] F.M. Ernsberger, *J. Non-Crystalline Solids* 25 (1977) 293.
- [37] B.R. Lawn and T.R. Wilshaw, *Fracture of Brittle Solids* (Cambridge, London, 1975), ch. 4.
- [38] M. Imaoka and I. Yasui, *J. Non-Crystalline Solids* 22 (1976) 315.
- [39] D.B. Marshall and B.R. Lawn, *J. Mat. Sci.*, in press.
- [40] B.R. Lawn and D.B. Marshall, in: *Fracture Mechanics of Ceramics*, eds. R.C. Bradt, D.P.H. Hasselman and F.F. Lange (Plenum, New York, 1978), vol. 3.
- [41] A.G. Evans, in: *Fracture Mechanics of Ceramics*, eds. R.C. Bradt, D.P.H. Hasselman and F.F. Lange (Plenum, New York, 1978), vol. 3.
- [42] M.V. Swain, in: *Fracture Mechanics of Ceramics*, eds. R.C. Bradt, D.P.H. Hasselman and F.F. Lange (Plenum, New York, 1978), vol. 3.